DOI:10.1190/segam2020-3419351.1

High-resolution velocity model building and least-squares imaging offshore Canada: a deep-water Orphan basin example

Tiago Alcantara, Eric Frugier and Bruno Virlouvet, PGS

Summary

A 500km^2 proof-of-concept project in deep-water Canada demonstrated the benefits of combining recently acquired multisensor streamer data and new imaging technologies to produce a detailed velocity model and a robust seismic image that can minimize uncertainties prior to drilling. We describe the full waveform inversion (FWI) and least-squares migration (LSM) workflow that not only resulted in high-resolution seismic sections, with improved fault definition and signal to noise (S/N) ratio in the Cretaceous and Jurassic sections, but also produced AVO-compliant image gathers that can benefit quantitative interpretation.

Introduction

The Tablelands 3D seismic survey is located in the eastern part of the Orphan basin, offshore Canada. The area is under-explored and seismic images suggest the presence of Jurassic source rocks, as well as hydrocarbon entrapments in the Tertiary, Cretaceous and upper Jurassic sections (Enachescu et al., 2010).

The combination of new broadband multisensor seismic data and imaging technology is crucial to develop this under-explored region. These data, rich in low and high frequency information, were used to estimate elastic parameters that are required to differentiate the rock properties and fluid content of potential reservoirs. FWI and LSM can exploit broadband data to estimate a detailed velocity field and produce a robust image of the subsurface that can minimize drilling risks and support reservoir characterization.

In this case study, both inversion methods were applied around the Great Barasway F-66 well (Figure 1). This area is characterized by small-scale Tertiary channel systems that distort the wavefield and introduce uncertainty through structural undulations, unreliable amplitude variations, and limited resolution.

Initial velocity model building

Tarantola (1984) and Mora (1987) described the seismic inversion experiment as a simultaneous migration and reflection tomography. In this experiment, reflection amplitudes were resolved by the high wavenumber component (reflectivity), while the prestack hyperbola shape and positioning are controlled by the low wavenumber component (velocity model). In this context, to proper invert for the high wavenumbers, the low wavenumber component must be properly resolved; otherwise the reflectivity inversion will be affected by cycle-skipping.

We used raw hydrophone data to estimate the low wavenumber component through a combination of ray-based wavelet shift tomography (Sherwood et al., 2011) and

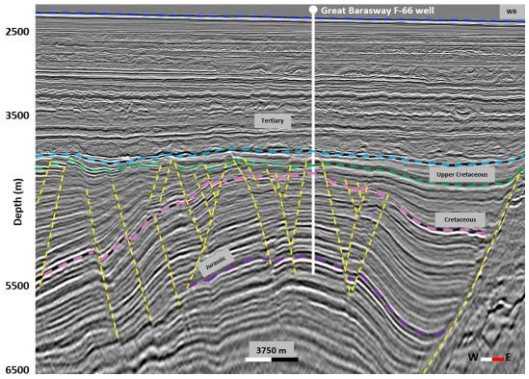

Figure 1. Great Barasway F-66 context. The well was drilled on a structural high with AVO anomaly.

a unique implementation of FWI (Ramos-Martinez et al., 2016).

The initial velocity model was built from prestack time migration velocities and horizons. It was then updated using ray-based tomography, resulting in a smooth velocity field that flattens the gathers while maintaining a reasonable correlation with the well information.

Additionally, to ensure the updated velocities could be used as a starting point to FWI, forward modeling was performed to confirm the mismatch between synthetic and recorded data was no greater than half of the dominant period.

Full waveform inversion

FWI is a nonlinear problem that generates high-resolution

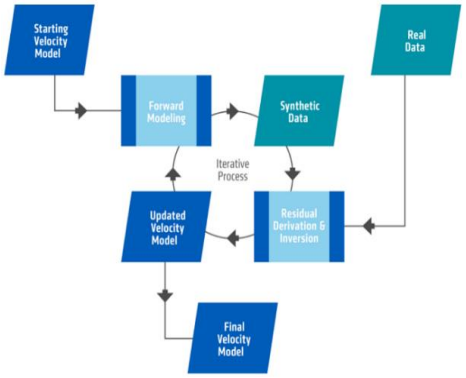

Figure 2. Full waveform inversion workflow.

velocity models by minimizing the misfit between observed and modeled shot data (Figure 2).

DOI:10.1190/segam2020-3419351.1

While conventional FWI relies on inverting for the refracted waves, the FWI implementation used in this example exploits the full wavefield and is able to update the velocity field beyond the penetration depth of the diving waves (Ramos-Martinez et al., 2016). This is particularly important in deep-water environments where refracted energy information is limited due to a lack of long offsets.

Modeling was performed using the acoustic, two-way wave equation with pseudo-analytical extrapolation in the time domain. The inversion uses a normalized form of the Born scattering kernel to compute the FWI gradient (Tarantola, 1984) through a variation of an inverse scattering imaging condition (ISIC). This gradient eliminates the migration isochrones that would generate high wavenumber artifacts characteristic to conventional cross-correlation FWI (Ramos-Martinez et al., 2016).

FWI relies on three key components: a wavelet, shot gathers and an initial velocity model. For this particular work, minimum phase, minimally processed raw hydrophone data was used in conjunction with a minimum phase wavelet and the ray-based tomographic velocity model previously mentioned.

In order to reduce the risk of cycle skipping while inverting for higher frequencies, a phase analysis was performed on denoised data to determine the minimum usable frequency for the initial FWI iterations. The result of this analysis indicated that 4Hz was adequate to start the inversion.

After defining the starting frequency, the velocity model was recursively updated using increasing frequency band from 4 to 25Hz. For each bandwidth, the velocity model was updated so that the misfit between recorded and modeled shots was reduced. The process then iterated until the FWI cost function acceptably converged. The quality control (QC) metrics for convergence were based on both amplitude misfits and cross-correlation between modeled and field data.

After each bandwidth inversion, additional QC was performed in both the data and image domains to ensure that model resolution and migrated image were improved. Such QCs included comparison between modeled and observed shots, FWI velocity perturbation, migrated gathers, and stacks before and after the inversion.

The outcome of this FWI workflow was a high-resolution velocity model that flattened gathers (Figure 3), improved the match between synthetic and observed data (Figure 4), and conformed to small-scale geological features such as the ones in the deeper Tertiary section (2700 m depth slice in Figure 5c).

Least-squares imaging

Conventional imaging methods such as Kirchhoff and Reverse time migration (RTM) produce a blurred approximation of the subsurface reflectivity. The seismic resolution and amplitudes are affected by different factors ranging from acquisition parameters, earth properties, and

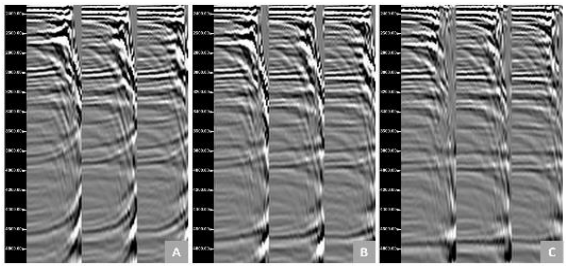

Figure 3. Offset domain common image gathers using initial model (A), ray-based tomography (B) and FWI (C).

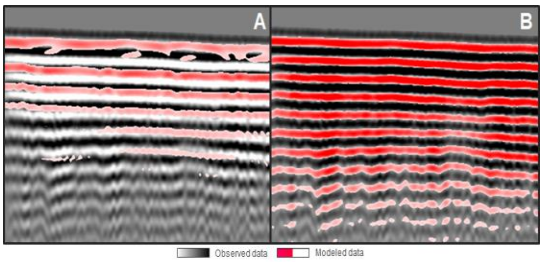

Figure 4. Match between modeled (red trough and no peak) and observed (white trough and black peak) common channel data before (A) and after FWI (B).

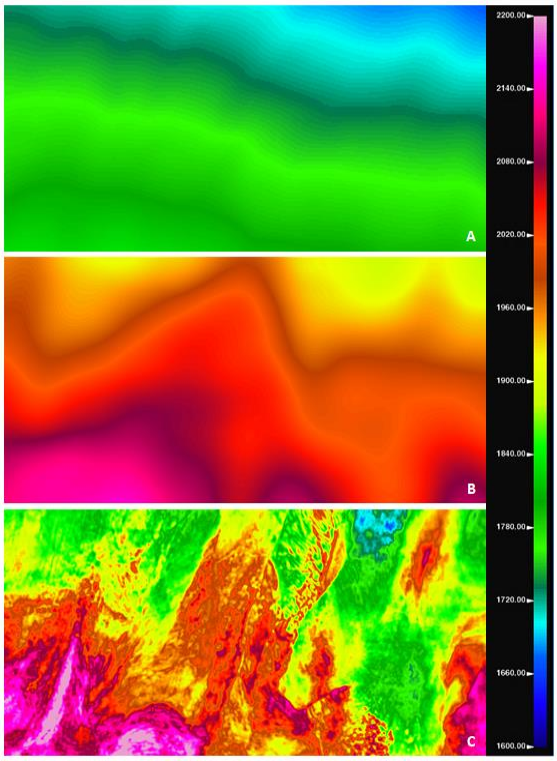

Figure 5. Initial velocity model (A), ray-based tomographic velocity model (B) and 25Hz FWI model (C) at depth slice 2700m.

the migration algorithm. In the presence of complex geology and non-optimum acquisition parameters, both illumination and wavenumber content of the migrated images are affected.

Least-squares migration can overcome these limitations by posing imaging as an inverse problem (Nemeth et al., 1999), thereby resulting in a better approximation of the earth's reflectivity. Different implementations of LSM exist in the industry; ranging from image-domain point spread functions (Valenciano, 2008) to data-domain approaches (Lu et al., 2017). Both implementations were used in this study.

Initially, an image-domain Kirchhoff LSM was used to obtain high-resolution AVO-compliant gathers. Later, a data-domain LSM using a visco-acoustic one-way wave equation operator was performed to enhance resolution and fault definition in the Cretaceous and Jurassic sections.

Image-domain least-squares migration

In image processing (Debnath et al., 2013), image blurring (equation 1) can be described as a convolution between the real object (x) and a distortion operator (A), plus some noise

$$b = Ax + n, \qquad (1)$$

(n). The distortion operator is also called the point spread function (PSF).

Image-domain LSM can be seen as a deblurring technique that attempts to recover the true reflectivity (x) by deconvolving an estimated distortion operator (A) from the migrated image b (Valenciano et. al, 2015; Klochikhina et al., 2016; Martin et al., 2019). Noise attenuation prior to the image restoration is necessary to avoid coherent noise (n) being boosted by deconvolution.

Image-domain LSM correspondingly starts with the PSF calculation. This two-step process consists of modeling and migrating a series of discrete point scatters (reflectivity) given the acquisition geometry and an accurate velocity field (ideally from FWI). Once computed, the PSFs are iteratively deconvolved from the migrated image yielding an improved representation of the reflectivity function (Figure 6).

In this study, Kirchhoff modeling and migration were performed to generate PSFs for 80 offsets. PSFs were deconvolved from denoised offset gathers to generate high-resolution, AVO-compliant gathers (Figure 7). Stacks were then created to analyze the improvements given by the inversion. Figure 8 shows that deblurring improved lateral and vertical resolution, yielding flatter and broader amplitude and frequency-wavenumber (FK) spectra. High wavenumber content corresponds to higher spatial resolution.

Data-domain least-squares migration

While image-domain LSM explicitly estimates and deconvolves PSFs from the migrated image, data-domain LSM implicitly solves for the reflectivity by means of an iterative data residual reduction (Arasanipalai et al., 2019; Korsmo et al., 2019). This methodology starts with synthetic shot generation (d_{syn}) through Born modelling using an accurate velocity model, an initial reflectivity (migrated image) and the acquisition geometry (shot gathers). A residual is estimated by minimizing the difference between

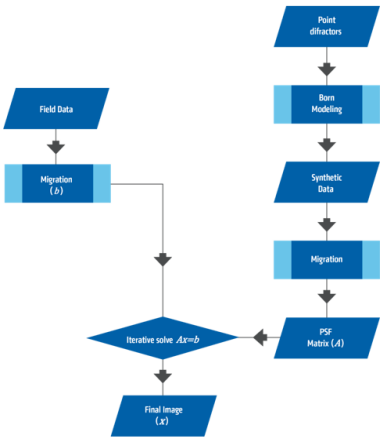

Figure 6. Image-domain least-squares migration workflow.

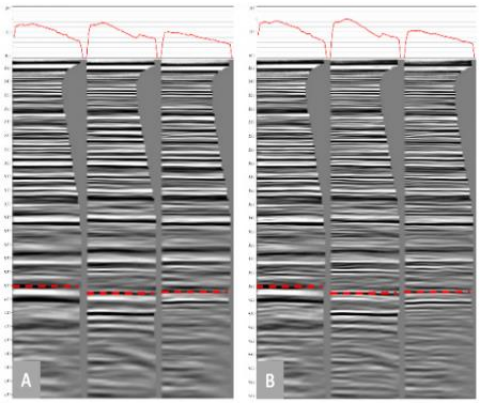

Figure 7. (a) Kirchhoff migrated; and (B) Kirchhoff LSM common image gathers with AVO extracted at the red dashed horizon.

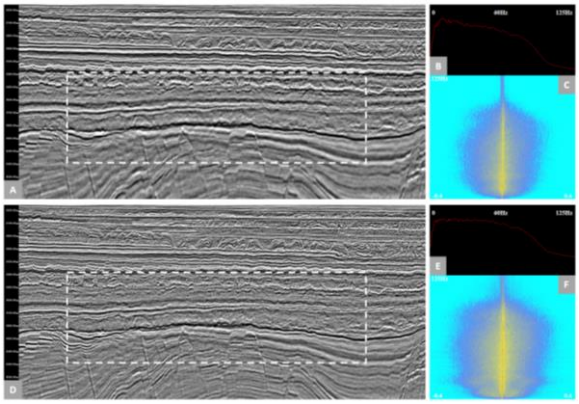

Figure 8. (A) Kirchhoff migrated; and (B) data domain LSM stacks. FK spectra were extracted in the white dashed window.

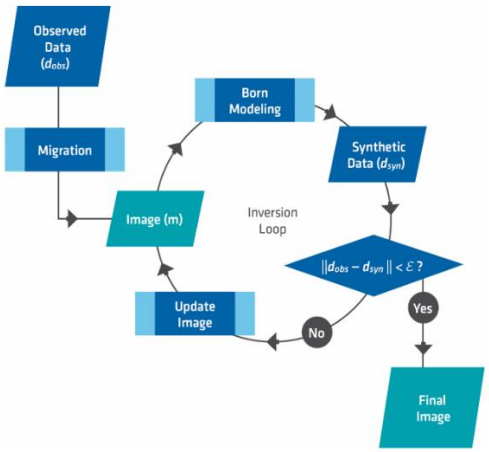

Figure 9. Data-domain LSM workflow.

the observed (d_{obs}) and synthetic data (d_{syn}). The image is then iteratively updated (Figure 9).

In this study, a 60Hz data-domain LSM used a visco-acoustic anisotropic one-way wave equation operator. This process used pre-processed shots gathers, the FWI velocity model and an initial reflectivity.

A comparison between migration (WEM and Kirchhoff) and the data-domain LSM shows that inversion sharpened faults, improved vertical resolution and enhanced signal to noise ratio (S/N) ratio in the Cretaceous and Jurassic sections (Figures 10 and 11), therefore resulting in a more detailed representation of the earth's reflectivity that can greatly benefit the exploration efforts.

Conclusions

New imaging technologies were applied to recently acquired multisensor deepwater streamer data from offshore Canada. This effort led to a robust subsurface image that can support new drilling opportunities in this frontier area.

FWI was instrumental in creating a detailed velocity model that explained the low wavenumber components of the data and enabled reflectivity inversion without cycle-skipping. An image-domain Kirchhoff LSM produced AVO-compliant image gathers with improved vertical and spatial resolution that benefit quantitative interpretation. Finally, a data-domain LSM using a one-way wave equation operator also yielded improvements in image resolution, fault definition and signal to noise ratio in the Cretaceous and Jurassic sections.

Therefore, the combination of multisensor streamer data and new imaging technologies leads to better seismic images and improved understanding of the petroleum system in this under-explored region.

Acknowledgements

We thank PGS for permission to publish this work. Furthermore, we thank Alejandro A. Valenciano, Jaime Ramos-Martinez, Samuel Brown and Alastair Lewis for their valuable discussions and support.

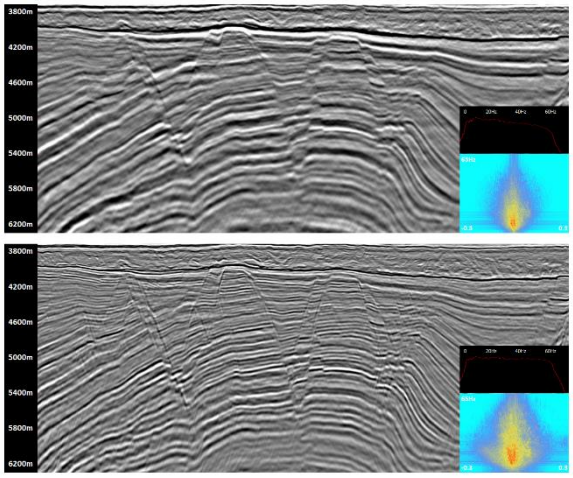

Figure 10. (A) 60Hz WEM; (B) data-domain LSM. Inversion (B) improves vertical resolution and fault definition compared to migration (A).

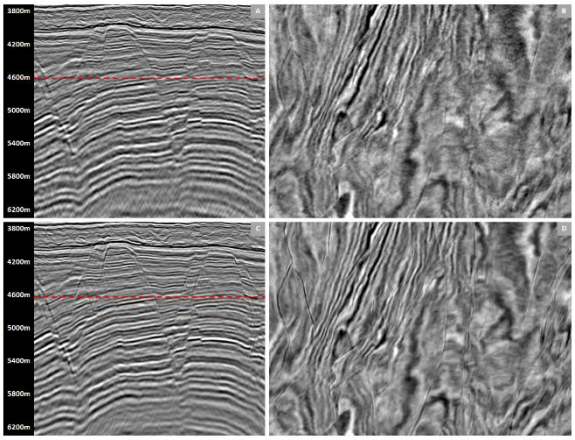

Figure 11. Kirchhoff (A and B) and data-domain LSM (C and D). Improved fault definition and S/N ratio in the inline direction (A and C). A depth slice at 4600m (B and D) shows the benefits aforementioned across the volume.

REFERENCES

Arasanipalai, S., H. Lebit, P. Ollagnon, B. Virlouvet, and J. Tilton, 2019, Enhanced presalt imaging using iterative least-squares migration: A case study in Santos Basin, Brazil: 89th Annual International Meeting, SEG, Expanded Abstracts, 4216–4220, doi: https://doi.org/10.1190/segam2019-3214351.1.

Debnath, A., H. Rai, C. Yadav, and A. Agarwal, 2013, Deblurring and denoising of magnetic resonance images using blind deconvolution method: Journal of Computer Applications, **81**, 7–12, doi: https://doi.org/10.5120/14046-2209.

Enachescu, M., I. Atkinson, J. Hogg, D. McCallum, and C. Rowe, 2010, Kimmeridgian source rock superhighway in the North Atlantic: Annual Convention and Exhibition, AAPG, Expanded Abstracts.

Klochikhina, E., S. Lu, A. A. Valenciano, and N. Chemingui, 2016, Subsalt imaging by wave equation reflectivity inversion: 78th Conference and Exhibition, EAGE, Extended Abstracts, Th SRS1 15.

Korsmo, Ø, S. Arasanipalai, and Z. Greplowski, 2019, Application of iterative least-squares migration in different geological settings: 81st Conference and Exhibition, EAGE, Extended Abstracts, We_R04_11.

Lu, S., X. Li, A. A. Valenciano, N. Chemingui, and C. Cheng, 2017, Least-squares wave-equation migration for broadband imaging: 79th Conference and Exhibition, EAGE, Extended Abstracts, Tu A1 07.

Martin, T., M. Barbaray, G. Venfield, and V. Chavda, 2019, Innovative inversion schemes for model building and reflectivity estimation: A deep water West African case study: 81st Conference and Exhibition, EAGE, Extended Abstracts, Tu_P01_01.

Mora, P., 1987, Nonlinear 2D elastic inversion of multi-offset seismic data: Geophysics, **52**, 1211–1228, doi: https://doi.org/10.1190/1.1442384.

Nemeth, T., C. Wu, and G. Schuster, 1999, Least-squares migration of incomplete reflection data: Geophysics, **64**, 208–221, doi: https://doi.org/10.1190/1.1444517.

Ramos-Martinez, J., S. Crawley, Z. Zou, A. A. Valenciano, L. Qui, and N. Chemingui, 2016, A robust gradient for long wavelength FWI updates: 78th Conference and Exhibition, EAGE, Extended Abstracts, Th SRS2 03.

Sherwood, J., J. Jiao, H. Tieman, K. Sherwood, C. Zhou, C. S. Lin, and S. Brandsberg-Dahl, 2011, Hybrid tomography based on beam migration: 81st Annual International Meeting, SEG, Expanded Abstracts, 3979–3983, doi: https://doi.org/10.1190/1.3628037.

Tarantola, A., 1984, In version of seismic data in the acoustic approximation: Geophysics, **49**, 1259–1266, doi: https://doi.org/10.1190/1.1441754.

Valenciano, A. A., 2008, Imaging by wave-equation inversion: Ph.D. thesis, Stanford University.

Valenciano, A. A., S. Lu, N. Chemingui, and J. Yang, 2015, High resolution imaging by wave equation reflectivity inversion: 77th Conference and Exhibition, EAGE, Extended Abstracts, We N103 15.